



# THE UNIVERSITY *of* EDINBURGH

## Edinburgh Research Explorer

### Darcy's law without friction in active nematic rheology

**Citation for published version:**

MacKay, F, Toner, J, Morozov, A & Marenduzzo, D 2020, 'Darcy's law without friction in active nematic rheology', *Physical Review Letters*. <https://doi.org/10.1103/PhysRevLett.124.187801>

**Digital Object Identifier (DOI):**

[10.1103/PhysRevLett.124.187801](https://doi.org/10.1103/PhysRevLett.124.187801)

**Link:**

[Link to publication record in Edinburgh Research Explorer](#)

**Document Version:**

Peer reviewed version

**Published In:**

Physical Review Letters

**General rights**

Copyright for the publications made accessible via the Edinburgh Research Explorer is retained by the author(s) and / or other copyright owners and it is a condition of accessing these publications that users recognise and abide by the legal requirements associated with these rights.

**Take down policy**

The University of Edinburgh has made every reasonable effort to ensure that Edinburgh Research Explorer content complies with UK legislation. If you believe that the public display of this file breaches copyright please contact [openaccess@ed.ac.uk](mailto:openaccess@ed.ac.uk) providing details, and we will remove access to the work immediately and investigate your claim.



# Darcy’s law without friction in active nematic rheology

Fraser Mackay<sup>1</sup>, John Toner<sup>2</sup>, Alexander Morozov<sup>1</sup>, Davide Marenduzzo<sup>1</sup>

<sup>1</sup>*SUPA, School of Physics and Astronomy, University of Edinburgh,  
Peter Guthrie Tait Road, Edinburgh EH9 3FD, UK*

<sup>2</sup>*Institute for Theoretical Sciences and Department of Physics, University of Oregon, Eugene, OR 97403, USA*

We study the dynamics of a contractile active nematic fluid subjected to a Poiseuille flow. In a quasi-1D geometry, we find that the linear rheology of this material is reminiscent of Darcy’s law in complex fluids, with a pluglike flow decaying to zero over a well-defined “permeation” length. As a result, the viscosity increases with size, but never diverges, thereby evading the yield stress predicted by previous theories. We find strong shear thinning controlled by an active Ericksen number quantifying the ratio between external pressure difference and internal active stresses. In 2D, the increase of linear regime viscosity with size only persists up to a critical length beyond which we observe active turbulent patterns, with very low apparent viscosity. The ratio between critical and permeation length, determining the stability of the Darcy regime, can be made indefinitely large by varying the flow aligning parameter or magnitude of nematic order.

Active gels provide a generic and universal model to understand the physics of active materials exerting non-thermal forces on the environment [1, 2]. Solutions of biopolymers, such as actin or microtubules, crosslinked by molecular motors, such as myosin or kinesin, are well described by the active gel paradigm [3, 4], and so are suspensions of self-motile microorganisms [5, 6]. According to the active gel theory, these systems can be modelled as a collection of force dipoles, exerted by the active particles (the motors or the microorganisms in the previous examples) on the surrounding fluid [1, 2]. Extensile active gels are those in which particles act on the surroundings via outward-pointing dipolar forces, contractile ones exert inward-pointing forces.

Theory [7–14] and experiments [15–17] have shown that active gels possess many intriguing and counter-intuitive flow and rheological properties, making them good candidates as new soft functional materials. Extensile fluids flow more easily due to activity, and can behave as “superfluids” with near-zero viscosity [7–11, 16, 17]. Contractile gels flow instead more *slowly* due to activity [7, 10, 15]. Theory suggests that the rheology of contractile active gels is reminiscent of that of glasses: these systems should be shear thinning and possess a yield stress when in the nematic phase [12]. Whilst numerical simulations of contractile active gels in the isotropic phase showed that their viscosity tends to infinity as the system approaches the spinodal point [8], whether or not the system should have a yield stress deep in the nematic phase is currently unclear. Here, the complication is that splay fluctuations are known to generically destroy nematic order in a large enough contractile system [18, 19], rendering calculations based on spatially homogeneous states inconclusive.

To address the yield stress issue, and to provide a complete theory for active contractile rheology, here we combine computer simulations and analytics to study contractile nematics subjected to a pressure-driven (Poiseuille) flow (Fig. 1a). We define an apparent viscos-

ity as in experiments, by analysing the magnitude of the throughput flow as a function of the forcing. Focussing initially on systems that do not flow spontaneously and on a “quasi-1D” geometry (in which order parameter and flow field vary in only one direction), we find no yield stress behaviour, but instead a viscosity which – in the linear regime – increases with sample size. The phenomenology of the associated flow, in particular the flow velocity profile and high apparent viscosity, is strikingly similar to permeation in liquid crystals [20–23] and to Darcy’s flow [25], but occurs here in the absence of any substrate friction. Our theory shows that this behaviour arises because active forces create a flow opposing that imposed by the pressure gradient, in a way which resembles friction qualitatively resulting in pluglike flow. In 2D or 3D systems, the Darcy-like flow persists only up to a critical length, beyond which we find chaotic behaviour, or “active turbulence” [5, 6, 26–29], with much lower viscosity. Importantly, we find that by changing the flow alignment angle and the amplitude of the nematic order parameter, the range of lengthscales over which the Darcy-like regime is stable can be increased without bound. This happens in particular when the amplitude of the nematic order parameter approaches zero [30].

To describe the equilibrium behaviour of our active nematic fluid, we used a particular Landau-de Gennes free energy  $\mathcal{F}$  with density  $f$  [31], which has two contributions. The first is a bulk term, which describes the isotropic-nematic transition:

$$f_1 = \frac{A_o}{2} \left( 1 - \frac{\gamma}{3} \right) Q_{\alpha\beta}^2 - \frac{A_o\gamma}{3} Q_{\alpha\beta} Q_{\beta\gamma} Q_{\gamma\alpha} + \frac{A_o\gamma}{4} (Q_{\alpha\beta}^2)^2. \quad (1)$$

The second term quantifies the cost of elastic distortions in the nematic orientation; in the one elastic constant approximation [32], it reads:

$$f_2 = \frac{K}{2} (\partial_\alpha Q_{\beta\gamma})^2. \quad (2)$$

In Eqs. (1) and (2),  $A_o$  is the bulk energy scale,  $\gamma$  is a

temperature-like parameter with an isotropic-to-nematic transition at  $\gamma = 2.7$ ,  $K$  is the elastic constant and  $\mathbf{Q}$  is the tensorial order parameter measuring orientational order [32]. We use the repeated index summation convention throughout, with Greek indices denoting Cartesian components.

The equation of motion for  $\mathbf{Q}$  is

$$\left(\frac{\partial}{\partial t} + u_\gamma \partial_\gamma\right) Q_{\alpha\beta} - S_{\alpha\beta}(\mathbf{Q}, \mathbf{W}) = \Gamma H_{\alpha\beta}, \quad (3)$$

where the first term on the left hand side describing the advection of rods by a fluid with velocity  $\mathbf{u}$ . The second term is a tensor that couples the rotation and stretching of the liquid crystals to the flow and has the form

$$\mathbf{S}(\mathbf{Q}, \mathbf{W}) = (\xi \mathbf{D} + \mathbf{\Omega})(\mathbf{Q} + \mathbf{I}/3) + (\mathbf{Q} + \mathbf{I}/3)(\xi \mathbf{D} - \mathbf{\Omega}) - 2\xi(\mathbf{Q} + \mathbf{I}/3)Tr(\mathbf{Q}\mathbf{W}), \quad (4)$$

where  $\mathbf{D} = (\mathbf{W} + \mathbf{W}^T)/2$  and  $\mathbf{\Omega} = (\mathbf{W} - \mathbf{W}^T)/2$  are the symmetric and anti-symmetric parts of the velocity gradient tensor  $W_{\alpha\beta} = \partial_\beta u_\alpha$  and  $\mathbf{I}$  is the identity matrix. The quantity  $\xi$  is the flow aligning parameter, which will play an important role in this work. Finally,  $\Gamma$  is the rotational diffusion constant, and the tensor  $\mathbf{H}$  is the molecular field,  $\mathbf{H} = -\frac{\delta \mathcal{F}}{\delta \mathbf{Q}} + \frac{1}{3}Tr\frac{\delta \mathcal{F}}{\delta \mathbf{Q}}$ .

The evolution of the fluid velocity field  $\mathbf{u}$  is described by the Navier-Stokes equation,

$$\rho(\partial_t + u_\beta \partial_\beta) u_\alpha = f_\alpha + \eta_0 \nabla^2 u_\alpha + \partial_\beta \Pi_{\alpha\beta}, \quad (5)$$

where  $\rho$  is the fluid density and  $f_\alpha$  is the externally applied pressure gradient. The fluid is assumed to be incompressible. The second term on the right hand side describes the viscous forces, where  $\eta_0$  is the background fluid viscosity, and  $\Pi_{\alpha\beta}$  is the stress tensor [7, 18, 26],

$$\begin{aligned} \Pi_{\alpha\beta} = & -P_0 \delta_{\alpha\beta} + 2\xi \left( Q_{\alpha\beta} - \frac{1}{3} \delta_{\alpha\beta} \right) Q_{\gamma\mu} H_{\gamma\mu} \quad (6) \\ & - \xi H_{\alpha\gamma} \left( Q_{\gamma\beta} + \frac{1}{3} \delta_{\gamma\beta} \right) - \xi \left( Q_{\alpha\gamma} + \frac{1}{3} \delta_{\alpha\gamma} \right) H_{\gamma\beta} \\ & - \frac{\partial f}{\partial (\partial_\beta Q_{\gamma\mu})} \partial_\alpha Q_{\gamma\mu} + Q_{\alpha\nu} H_{\nu\beta} - H_{\alpha\nu} Q_{\nu\beta} - \zeta Q_{\alpha\beta}, \end{aligned}$$

where the last term is the active stress. The activity  $\zeta$  is negative for contractile fluids, and positive for extensile systems. For more details see [33].

We begin by reporting lattice Boltzmann simulation results for the linear rheology of contractile fluids under Poiseuille flow (Fig. 1; see [24] for methods). We consider a quasi-1D active nematic (where orientational order and flow velocity only vary along  $z$ ) confined between two infinite parallel plates at  $z = 0$  and  $z = L_z$ , subject to a constant body force (magnitude  $f$ ) along  $y$ . The nematic order parameter  $\mathbf{Q}$  is pinned at the plates to  $\mathbf{Q}_0 = q(\hat{y}\hat{y} - \mathbf{I}/3)$ , where the magnitude  $q$  of the order parameter is determined by minimizing the bulk free energy density

in Eq. (1), which gives  $q = \frac{1}{4} \left( 1 + \sqrt{9 - \frac{24}{\gamma}} \right)$ . We also impose no-slip boundary conditions  $\mathbf{u} = \mathbf{0}$  at the plates.

We define an apparent viscosity  $\eta = \eta_0 M_0 / M$  in terms of the throughput flow of the active nematic, with  $M = \int_0^{L_z} dz v_y(z)$ , and  $M_0$  the value for a Newtonian fluid with viscosity  $\eta_0$  in a channel of the same width and subject to the same body force. The velocity profiles in the steady state are shown in Fig. 1b for different values of system size  $L_z$  (and the same value of  $f$ ). These correspond to the linear regime, so that further decreasing  $f$  leads to no changes in  $\eta$ . We find no sign of a yield stress. Notably, though, we find pluglike flow for all  $L_z$ , with near-uniform velocity in the bulk of the channel, and all the shear confined in a small region close to the wall (Fig. 1b). An analysis of the profiles in Fig. 1b shows that the maximum velocity scales as  $L_z$ , whereas the length-scale over which  $v_y$  drops to 0 (the ‘‘permeation length’’  $\lambda_p$ ) does not vary appreciably with size.

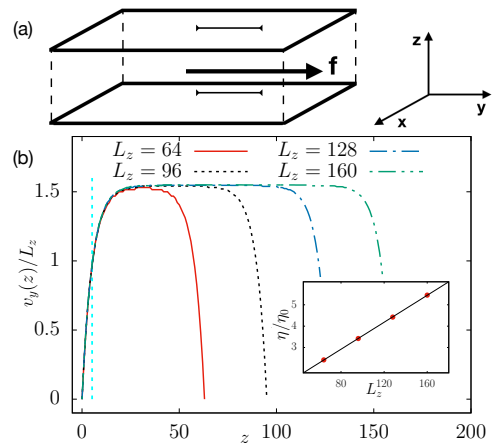


FIG. 1: (a) A schematic diagram of the channel with walls at the boundaries in the  $z$ -direction and periodic boundaries in  $x$  and  $y$ . A constant body force  $\mathbf{f}$  is applied in the positive  $y$ -direction. In our quasi-1D geometry  $Q$  and  $\mathbf{u}$  only depend on  $z$ ; in 2D simulations, they depend on  $y$  and  $z$ . (b) Numerical results showing the  $y$ -component of the velocity (scaled by system size) against  $z$  for systems of varying channel width. The permeation length  $\lambda_p$  has been determined by fitting these curves to the velocity field in Eq. 9 thus showing that  $\lambda_p$  (represented by the dotted vertical line) is independent of  $L_z$ . The inset shows a plot of  $\eta/\eta_0$  in the linear regime of contractile active liquid crystals in one-dimension against the channel width  $L_z$ .

To better understand these results, we linearise the steady state equations of motion for our quasi-1D case to obtain,

$$\begin{aligned} \Gamma K \delta Q'' + x_2 v' &= 0, \quad (7) \\ \eta_0 v'' - \zeta \delta Q' - x_2 K \delta Q''' + f &= 0, \end{aligned}$$

where  $x_2 \equiv (2\xi + q(\xi - 3))/6$  [24], whereas  $\delta Q = \delta Q_{yz}$  and  $v = u_y$  are the deviations of the order parameter tensor

and the flow field from their rest values ( $\mathbf{Q} = \mathbf{Q}_0$  and  $\mathbf{u} = \mathbf{0}$ ) due to the body force  $f$ . This set of equations – which is a valid approximation of the full model in the linear regime of  $f \rightarrow 0$  – is solved by:

$$\delta Q = \frac{fL_z}{2|\zeta|} \left( \frac{\sinh(\delta z/\lambda_p)}{\sinh(L_z/2\lambda_p)} - \frac{2\delta z}{L_z} \right), \quad (8)$$

$$v = \frac{K\Gamma f L_z \coth(L_z/2\lambda_p)}{2x_2\lambda_p|\zeta|} \left[ 1 - \frac{\cosh(\delta z/\lambda_p)}{\cosh(L_z/2\lambda_p)} \right] \quad (9)$$

with  $\delta z = z - L_z/2$ . The flow field in Eq. 9 corresponds to pluglike flow (Fig. 1b), with constant velocity except in a boundary layer of size  $\lambda_p = \sqrt{\frac{\Gamma\eta_0 K + 2Kx_2^2}{|\zeta|x_2}}$ . For  $\Gamma\eta_0$  sufficiently large, the permeation length  $\lambda_p \sim l_a \sqrt{\Gamma\eta_0}$ , where we have introduced the active lengthscale  $l_a = \sqrt{K/|\zeta|}$ . This scaling holds in our simulations (Fig. S1).

Integrating the velocity over the channel we obtain  $M = \int_0^{L_z} v dz$ . This leads to

$$\eta = \frac{L_z \lambda_p x_2 |\zeta|}{6\Gamma K \left[ \coth\left(\frac{L_z}{2\lambda_p}\right) - 2\frac{\lambda_p}{L_z} \right]}. \quad (10)$$

The apparent viscosity  $\eta$  tends to a constant for  $L_z \ll \lambda_p$ , and increases linearly with  $L_z$  for  $L_z \gg \lambda_p$ , as found numerically (Fig. 1b, inset). Our theory shows that the nontrivial behaviour is due to the pluglike flow velocity profile, which occurs here *despite* the absence of a frictional substrate. This is reminiscent of Darcy’s flow in porous media [25], or of permeative flows in cholesteric liquid crystals [22, 23]. We therefore refer to this linear regime of contractile fluids as the “Darcy” regime. A Darcy-like flow appears because Eq. 7 implies that  $\delta Q'' \propto v'$  in steady state, so that the terms dependent on  $\delta Q'$  in Eq. (8) introduce, among others, a term linear in  $v$ , which is formally similar to the contribution describing friction with a substrate. Physically, the mechanism underlying the onset of a Darcy-like pluglike flow is that the active flow due to the non-trivial order parameter profile pulls back on the fluid and opposes the externally imposed flow. This results in the removal of gradients in the order parameter and velocity in the bulk.

To address the stability of the Darcy regime as a function of the pressure gradient, we now study the nonlinear rheology of active contractile nematics. Inspection of Eq. 5 suggests that in steady state we may expect a balance between the body force and the divergence of the stress tensor. The latter should be dominated by the active contribution  $\sim |\zeta|$  [7]. Dimensional analysis then yields  $\tilde{f} = fl/|\zeta|$  as a potential control parameter, which determines the relative weight between external forcing and internal active stresses; we call this an active Ericksen number. Here,  $l$  is a length quantifying the scale over which the active stress and orientation order vary spatially – in our simulations, we find the relevant lengthscale to be  $L_z$ , hence  $\tilde{f} = fL_z/|\zeta|$ .

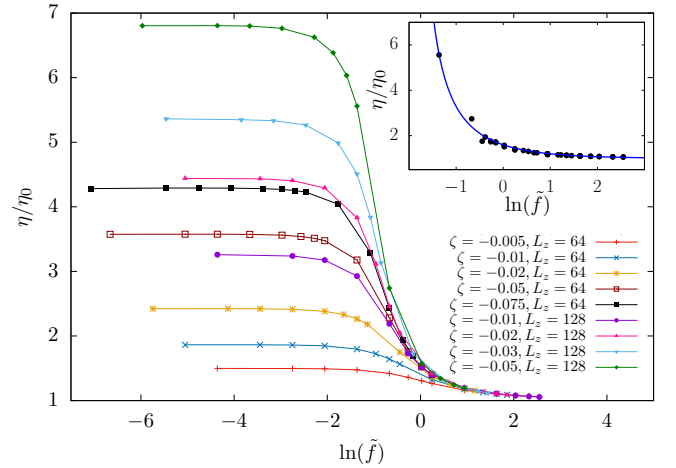


FIG. 2: Plot of  $\eta/\eta_0$  against  $\ln(\tilde{f})$ , from numerical simulation of a quasi-1D contractile active material. At lower  $\tilde{f}$ ,  $\eta/\eta_0$  is constant and increases with the channel width. The inset shows a fit to  $\frac{1+b\tilde{f}}{b\tilde{f}-c}$ , with  $b, c > 0$ .

Figure 2 plots the apparent viscosity found in simulations as a function of  $\tilde{f}$ . We find that all the curves collapse as a function of  $\tilde{f}$ , whereas they diverge for sufficiently large values of  $\tilde{f}$ , whereas they diverge for small forcing (to yield the linear regime apparent viscosity discussed in Fig. 1). In other words, there is a crossover between the Darcy regime and a universal shear thinning regime, which is singly determined by  $\tilde{f}$ . The dependence of the apparent viscosity on  $\tilde{f}$  can be understood via a qualitative scaling argument which adds the Newtonian and the opposing active contribution to the throughput flow  $M$ , as shown in [24].

The quasi-1D approximation described above is useful as it allows a complete characterisation of the rheology of a contractile gel, together with an analytically tractable theory which uncovers the mechanism leading to a Darcy-like linear regime with no yield stress. However, the persistence of the Darcy regime to arbitrarily large system size which we observe in Fig. 1 is due to the special features of our effectively 1D geometry [26, 34]. In a fully 2D or 3D system, we only expect the Darcy regime to be stable up to a finite system size, as it has long been known [18] that infinitesimal splay fluctuations destabilise the uniform state of the contractile active nematic for  $L_z > L_c$  – an instability lengthscale proportional to  $l_a$ .

To explore the more general problem of 2D contractile rheology, we now use simulations to study the case in which the  $\mathbf{Q}$  tensor and velocity fields depend on both  $y$  and  $z$  (though orientational order and flow can also point out of the  $(y, z)$  plane) [35]. We focus on the case of a fixed (small) value of  $f$ . Fig. 3(a) shows  $\eta$  as a function of system size  $L_z$ . As anticipated, the Darcy-like regime (corresponding to the increase of  $\eta$  with  $L_z$ ) gives way to another regime – characterised by much smaller viscosity

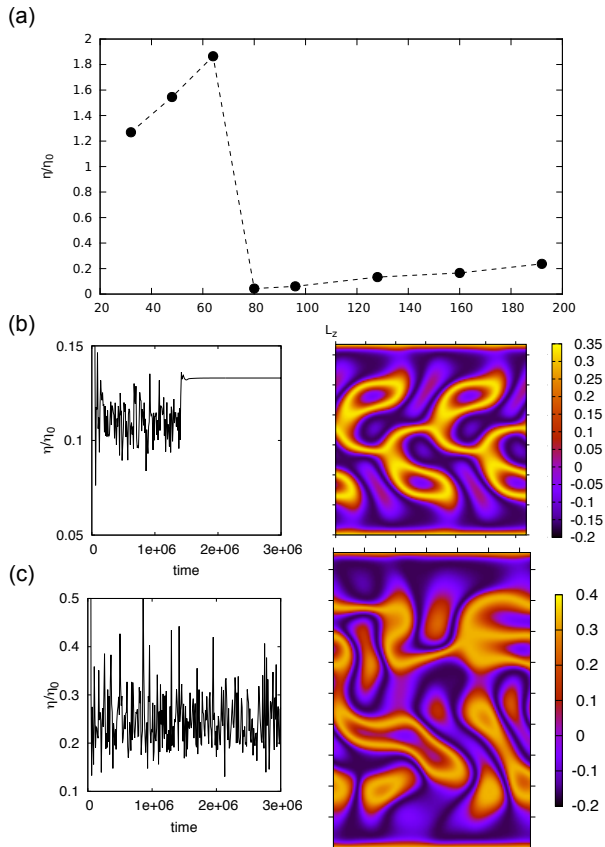


FIG. 3: (a) A plot of  $\eta/\eta_0$  against  $L \equiv L_z$  for small fixed body force ( $f = 10^{-6}$ ) for contractile active nematics ( $|\zeta| = 0.01$ ). (b) Viscosity versus time (left) and  $Q_{yz}$  pattern (right) for a system with  $L_z = 128$ . (c) Viscosity versus time (left) and  $Q_{yz}$  pattern for a system with  $L_z = 192$ . Axes ticks in the right patterns in (b,c) are shown every 20 lattice sites.

– beyond the instability lengthscale  $L_c$ .

In the unstable regime, the apparent viscosity varies chaotically over time, so that the system is in the active turbulent regime, best characterised for extensile fluids [5]. Remarkably, we find that in several cases the chaotic dynamics settles into a spatially-dependent non-trivial travelling wave pattern – an example of the resulting  $Q$  tensor texture is shown in Fig. 3(b). The existence of multiple possible non-trivial travelling wave solutions is reminiscent of the phenomenology of low-dimensional models for Newtonian turbulence [36], although here these states appear to be linearly stable. The travelling wave states and turbulent patterns both involve a characteristic lengthscale, which in our simulations is close to the active lengthscale  $l_a$ , known to set the typical vortex size in active turbulence [33]. For sufficiently large  $\tilde{f}$ , we re-enter the 1D shear thinning pattern, as the forcing is strong enough to suppress variation along the flow direction (as for shear [37]; Fig. S2).

To complement our simulations, we calculated exactly

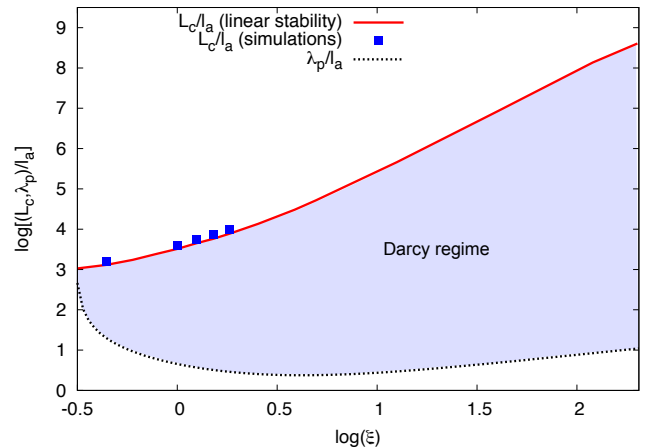


FIG. 4: Log-log plot of the instability lengthscale  $L_c$  (solid line, exact numerics, and filled squares, lattice Boltzmann) and of  $\lambda_p$  (dotted line) as a function of  $\xi$ , for  $A_0 = 1$ ,  $\gamma = 3$ ,  $q = 1/2$ ,  $\Gamma = 0.33775$ ,  $\eta_0 = 5/3$ ,  $K = 0.04$  and variable  $\zeta$ . Lengthscales are in units of  $l_a$ .

the value of  $L_c$  – beyond which the Darcy regime is unstable in 2D [35] with our boundary conditions – by using a spectral Chebyshev method [24, 38]. Figure 4 plots the dependence of  $L_c$  on  $\xi$ , and shows that increasing the flow aligning parameter leads to a dramatic enhancement of the stability range of the quasi-1D Darcy regime. By following [39], we can relate  $\xi$  to microscopic parameters accessible experimentally via the formula

$$\xi = \frac{2 \frac{I_L + 2I_s}{I_L - I_s} + q}{2 + q} \quad (11)$$

where  $I_L$  and  $I_s$  are, respectively, the largest eigenvalue of the moment of inertia tensor of the constituent nematogens, and the mean of the two smallest eigenvalues. Eq. (11) and Fig. 4 predict that, for instance,  $I_L/I_s = 4$  and  $q = 1/2$  give  $\xi = 1.8$ , for which  $L_c/\lambda_p \simeq 60$  (Fig. 4), corresponding to a large Darcy regime.

Another way to increase the stability range of the Darcy regime is to decrease the value of the nematic order  $q \rightarrow 0$  [24]. This limit could be reached in models in which the cubic term in Eq. (1) gets very small (for instance a theory for weakly ordered thin actomyosin films), or in mixtures of prolate and oblate molecules.

In summary, we have shown that an active contractile nematic subjected to a pressure-driven flow does not possess a yield stress, and evades it by instead acquiring a size-dependent viscosity associated with pluglike flow which is reminiscent of Darcy’s flow in porous materials. The Darcy regime is always found in a quasi-1D geometry (with variation of order and flow along a single direction) for sufficiently small values of the body force. In a 2D geometry, the Darcy regime is instead only observed up to a critical system size, beyond which we find chaos and active turbulence. The range of stability of the Darcy

regime in 2D is tunable, and can be increased virtually indefinitely by a suitable choice of parameters. In particular, our results suggest that this range can be very large in thin and weakly ordered films of actomyosin, for which  $l_a$  is a few microns [40]. We hope this prediction will stimulate experiments on channel flow in active contractile systems – such as, but not limited to, myosin-filament mixtures – aimed at observing all rheological regimes we predict here – Darcy flow, shear thinning and chaos.

We thank the Higgs Centre for Theoretical Physics for supporting two of JT's visits to the University of Edinburgh, during which part of this work was performed.

- 
- [1] S. Ramaswamy, *Annu. Rev. Condens. Matter Phys.* **1**, 323 (2010).
- [2] M. C. Marchetti, J.-F. Joanny, S. Ramaswamy, T. B. Liverpool, J. Prost, M. Rao, and R. A. Simha, *Rev. Mod. Phys.* **85**, 1143 (2013).
- [3] T. Sanchez, D. T. N. Chen, S. J. DeCamp, M. Heymann, and Z. Dogic, *Nature* **491**, 431 (2012).
- [4] M. S. e Silva, M. Depken, B. Stuhmann, M. Korsten, F. C. MacKintosh, and G. H. Koenderink, *Proc. Natl. Acad. Sci. USA* **108**, 9408 (2011).
- [5] H. H. Wensink, J. Dunkel, S. Heidenreich, K. Drescher, R. E. Goldstein, H. Löwen, and J. M. Yeomans, *Proc. Natl. Acad. Sci. USA* **109**, 14308 (2012).
- [6] A. Sokolov, I. S. Aranson, J. O. Kessler, and R. E. Goldstein, *Phys. Rev. Lett.* **98**, 158102 (2007).
- [7] Y. Hatwalne, S. Ramaswamy, M. Rao, and R. A. Simha, *Phys. Rev. Lett.* **92**, 118101 (2004).
- [8] M. E. Cates, S. M. Fielding, D. Marenduzzo, E. Orlandini, and J. M. Yeomans, *Phys. Rev. Lett.* **101**, 068102 (2008).
- [9] L. Giomi, T. B. Liverpool, and M. C. Marchetti, *Phys. Rev. E* **81**, 051908 (2010).
- [10] D. Saintillan, *Annu. Rev. Fluid Mech.* **50**, 563 (2018).
- [11] A. Loisy, J. Eggers, and T. B. Liverpool, *Phys. Rev. Lett.* **121**, 018001 (2018).
- [12] T. B. Liverpool and M. C. Marchetti, *Phys. Rev. Lett.* **97**, 268101 (2006).
- [13] D. Marenduzzo, E. Orlandini, and J. M. Yeomans, *Phys. Rev. Lett.* **98**, 118102 (2007).
- [14] S. M. Fielding, D. Marenduzzo, and M. E. Cates, *Phys. Rev. E* **83**, 041910 (2011).
- [15] S. Rafai, L. Jibuti, and P. Peyla, *Phys. Rev. Lett.* **104**, 098102 (2010).
- [16] H. M. López, J. Gachelin, C. Douarche, H. Auradou, and E. Clément, *Phys. Rev. Lett.* **115**, 028301 (2015).
- [17] V. A. Martinez *et al.*, *Proc. Natl. Acad. Sci. USA* **117**, 2326 (2020).
- [18] R. A. Simha and S. Ramaswamy, *Phys. Rev. Lett.* **89**, 058101 (2002).
- [19] S. Ramaswamy and M. Rao, *New J. Phys.* **9**, 423 (2007).
- [20] W. Helfrich, *Phys. Rev. Lett.* **23**, 372 (1969).
- [21] P. M. Chaikin and T. C. Lubensky, *Introduction to Condensed Matter Physics* (Cambridge University Press, 1995).
- [22] D. Marenduzzo, E. Orlandini, and J. M. Yeomans, *Phys. Rev. Lett.* **92**, 188301 (2004).
- [23] D. Marenduzzo, E. Orlandini, and J. Yeomans, *The Journal of chemical physics* **124**, 204906 (2006).
- [24] See Supplemental Material for details of our numerical scheme, additional results and a description of the exact numerics used to obtain the results in Fig. 4.
- [25] S. Whitaker, *Transport Porous Med.* **1**, 3 (1986).
- [26] D. Marenduzzo, E. Orlandini, M. E. Cates, and J. M. Yeomans, *Phys. Rev. E* **76**, 031921 (2007).
- [27] S. P. Thampi, R. Golestanian, and J. M. Yeomans, *Phys. Rev. Lett.* **111**, 118101 (2013).
- [28] C. Dombrowski, L. Cisneros, S. Chatkaew, R. E. Goldstein, and J. O. Kessler, *Phys. Rev. Lett.* **93**, 098103 (2004).
- [29] A. Sokolov and I. S. Aranson, *Phys. Rev. Lett.* **109**, 248109 (2012).
- [30] Since the isotropic-nematic transition is first order, there is usually a lower bound on the amplitude of  $q$ . However, as one approaches a prolate-oblate-biaxial nematic multicritical point (see R. Alben, *Phys. Rev. Lett.* **30**, 778 (1973)), the size of the first order jump vanishes. Hence, near such a multicritical point, which can be realized experimentally by mixing prolate and oblate molecules, it is possible to make the nematic order parameter arbitrarily small.
- [31] A. N. Beris and B. J. Edwards, *Thermodynamics of flowing systems: with internal microstructure* (Oxford University Press on Demand, 1994).
- [32] P. D. deGennes and J. Prost, *The Physics of Liquid Crystals* (Clarendon Press, 1993).
- [33] A. Doostmohammadi, J. Ignés-Mullol, J. M. Yeomans, and F. Sagués, *Nat. Comm.* **9**, 3246 (2018).
- [34] S. A. Edwards and J. M. Yeomans, *EPL* **85**, 18008 (2009).
- [35] Selected 3D lattice Boltzmann simulations suggest that  $L_c$  is the same in 2D and 3D.
- [36] F. Waleffe, *Phys. Fluids* **9**, 883 (1997).
- [37] S. Muhuri, M. Rao, and S. Ramaswamy, *EPL* **78**, 48002 (2007).
- [38] C. Canuto, M. Hussaini, A. Quarteroni, and T. Zang, *Spectral Methods in Fluid Dynamics*, Springer, Berlin (1988).
- [39] D. Forster, *Phys. Rev. Lett.* **32**, 1161 (1974).
- [40] M. Nishikawa, S. R. Naganathan, F. Julicher, *eLife* **6**, e19595 (2017).